Phase and structural characterization of phosphate-tellurite crystalline materials

M. ELISA[a], I. C. VASILIU[a], B. A. SAVA[b], L. BOROICA[b], A. V. FILIP[b,*], M. C. DINCA[b], C. BARTHA[c]
[a]*Optospintronics Department, National Institute of R & D for Optoelectronics-INOE 2000, 409 Atomistilor Str., 077125, Magurele, Ilfov, Romania*
[b]*Lasers Department, National Institute for Laser, Plasma and Radiation Physics, 409 Atomistilor Str, 077125 Magurele, Ilfov, Romania*
[c]*Magnetism and Superconductivity Laboratory, National Institute of Materials Physics, 405 A Atomistilor Str, 077125 Magurele, Ilfov, Romania*

Phosphate-tellurite crystalline materials containing titanium and aluminum oxide as well as a tellurite crystalline material containing lithium, barium and aluminum oxide were synthesized and investigated by X-ray diffraction (XRD) and Fourier Transform Infrared (FTIR) spectroscopy. XRD analysis shows peaks specific to the crystalline phases $Al(PO_3)_3$ and TiP_2O_7. FTIR analysis revealed absorption bands specific to the bending and stretching vibration modes of the phosphate and tellurite crystalline networks.

(Received February 17, 2021; accepted June 11, 2021)

Keywords: Phosphate compounds, Tellurite compounds, Glass ceramics, X-ray Diffraction, FTIR analysis

1. Introduction

Phosphate, tellurite, and phosphate-tellurite glass ceramics have attracted high interest due to their applications in optics, optoelectronics, magneto-optics and nuclear domains. In the following, a brief survey of the recent studies is presented.

Thus, current investigations have been achieved on the crystallization of rare-earth-doped phosphate glasses. Thus, Yb-doped sodium NaF phosphate glass-ceramics were reported and crystalline phases as $NaPO_3$, $Na_5P_3O_{10}$ and $NaYbP_2O_7$ were formed after the heat treatment of the parent glass [1]. These glass-ceramic materials are applied for solid-state lasers.

The influence of Al_2O_3 and Y_2O_3 addition on the crystallization and luminescence of a Yb-doped sodium strontium phosphate glass was explored [2]. The crystallization of the $NaYbP_2O_7$ phase increases the luminescence lifetime and the emission of Yb^{3+} ions, these materials having to attract applications for optical fibre lasers and amplifiers.

In the glass system Na_2O-CaO-CaF_2-P_2O_5 doped with Er^{3+}, the influence of the composition as well as of the heat treatment temperature was investigated in order to promote the CaF_2 crystalline phase formation, with application in telecommunications [3].

Eu/Nd/La-doped phosphate glass-ceramics from the system K_2O-BaO-Al_2O_3-NaF-K_2O_5 have been synthesized and annealed in order to promote the crystalline phase nucleation and growth: $KBa_2(PO_3)_5$, Ba_5P_9, $BaNd_2O_4$, $K(PF_6)$, $Ba(AlF_5)$, $Na_4Ba(PO_3)_6$ and $AlPO_4$ for lasers applications [4].

Iron zinc phosphate glass-ceramics have been synthesized being used for nuclear waste immobilization due to the high capability of the vitreous phosphate host to bond different chemical compounds. Several crystalline phases were found such as $Zn_2P_2O_7$, $Zn(PO_3)_2$ and $ZnFe_2O_4$ [5].

Other phosphate glass-ceramics containing Na_2O, Fe_2O_3 and Al_2O_3 have been prepared in order to embed nuclear wastes composed of lanthanide ions [6]. The crystalline phases are composed of monazite (orthophosphates of lanthanide ions) and orthophosphate of Na, Al and Fe.

Different phosphate glasses containing iron, lead and zinc have been investigated in relation to the crystallization tendency [7]. Certain crystalline phases $Fe_3(P_2O_7)_2$, $Fe_4(P_2O_7)_3$ and $Fe(PO_3)_3$, $Fe_7(PO_4)_6$, $Fe_2Pb_3(PO_4)_4$ were formed having application as glass-ceramic materials for nuclear waste neutralization.

Rare-earth-doped tellurite glass-ceramics have been synthesized due to their enhanced magnetic and optical properties. Recently, new Co-doped lithium zirconium tellurite glass-ceramics have been reported for their applications as sensors and magneto-optical devices related to $CoTeO_3$ crystalline phase formation [8].

The influence of Ag and Cu nanoparticles as well as of $TbTe_6O_{15}$ crystalline phase on the luminescence and magnetic behaviour of terbium lead tellurite glass-ceramics have been investigated [9].

CaF_2 nanocrystals have been explored in an alumina NaF-CaF_2 tellurite glass having applications in the field of optical modulators and optical storage systems [10].

Transparent niobium bismuth tellurite glass-ceramics were obtained by a controlled crystallization process of a

starting glass, presenting a long-scale transmission up to 5.5 µm [11]. Nb_2O_5 and Bi_2O_3 improve the mechanical and thermal properties of the glass-ceramics.

Very recently, transparent glass ceramics from the system Na^+/Eu^{3+}-co-doped $CaO-WO_3-SiO_2$ has been synthesized in order to promote the crystallization process [12]. The luminescence properties of the glass ceramics have been investigated.

Aluminum barium titanate glass ceramic composites have been prepared for dielectric properties and the crystallization temperature has been explored [13].

Phosphate-tellurite glass-ceramic materials have been recently studied for their applications in optical amplifiers and solid-state lasers. Thus, $ErPO_4$ nanocrystals were formed from a starting Er-doped zinc sodium phosphate-tellurite glass by appropriate heat treatment [14].

Er^{3+}-doped phosphate-tellurite fluoride glass-ceramics have been synthesized to provide BaF_2 nanocrystals embedded in the vitreous phase. The final transparent glass-ceramics were investigated for middle infrared (MIR), near-infrared (NIR) and up-conversion (UC) luminescence by comparison with the initial doped glass [15].

In the present work, crystalline phosphate-tellurite materials have been synthesized, the phase composition and structure being analysed for potential heat resistance and insulation applications. This study intended to establish a correlation between the oxide composition, synthesis parameters, crystalline phase formation, size of the nanocrystals and optical phonons specific to the phosphate-tellurite network. This study presents the oxide composition, synthesis parameters, crystalline phase formation, size of the nanocrystals and optical phonons specific to some phosphate-tellurite crystalline materials containing aluminum and titanium oxides.

2. Experimental

Phosphate-tellurite crystalline materials have been synthesized by a non-conventional wet-route, starting with the homogenization-evaporation of water and CO_2 from the chemical precursors, followed by melt-quenching step, as it is presented in the case of a titanium phosphate-tellurite glass and zinc phosphate-tellurite glass [16-18]. The nominal oxide composition (mol. %) of the prepared crystalline materials is presented in Table 1. As shown in Table 1, the phosphate-tellurite samples contain Al_2O_3 and TiO_2 and a constant proportion of TeO_2.

Table 1. Synthesis parameters of the phosphate-tellurite crystalline materials

Glass code	Nominal oxide composition (mol. %)	Preliminary heat treatment parameters	Heat treatment parameters	Aspect
Te-1	$10TiO_2$-$20Al_2O_3$-$65P_2O_5$-$5TeO_2$	Homogenization & evaporation at 200°C, for 30 min, followed by heat treatment at 700°C, for 5 h	1200°C, for 30 min	White, crystallized, opaque material, adhering to the ceramic crucible
Te-2	$10TiO_2$-$10Al_2O_3$-$75P_2O_5$-$5TeO_2$	Homogenization & evaporation at 200°C, for 60 min, followed by heat treatment at 700°C, for 4.5 h	1200°C, for 15 min	White, crystallized, opaque material, adhering to the ceramic crucible
Te-3	$5TiO_2$-$20Al_2O_3$-$70P_2O_5$-$5TeO_2$	Homogenization & evaporation at 200°C, for 30 min, followed by heat treatment at 700°C, for 4.5 h	1200°C, for 75 min	Red, crystallized, opaque material, adhering to the ceramic crucible

The X-ray diffraction (XRD) measurements were performed at room temperature, in the 10° to 80° range, with 0.05° step and 3s integration time, using a Bruker D8 Advance device (CuKα, λ = 1.54056 Å). ICDD Powder Diffraction Files database [19] was used to identify the crystalline phases.

Fourier Transform Infrared (FTIR) spectroscopy measurements were carried out at RT, in the range 400-1500 cm^{-1}, using a Perkin Elmer BX Spectrum-Pike spectrometer in Transmission and Attenuated Total Reflection (ATR, ZnSe/Germanium window) modes.

3. Results

Figs. 1a, b, c present the XRD patterns of Te-1, Te-2, and Te-3 phosphate-tellurite samples.

The average crystallite size of each sample was estimated from Scherrer's equation displayed below:

$$D = \frac{k\lambda}{\beta cos\theta} \quad (1)$$

where K is a dimensionless shape factor (with a value of about 0.9), λ is the wavelength of the X-ray beam (CuKα, λ = 1.54056 Å), β is the line broadening at half of the maximum intensity and θ is the Bragg angle [20].

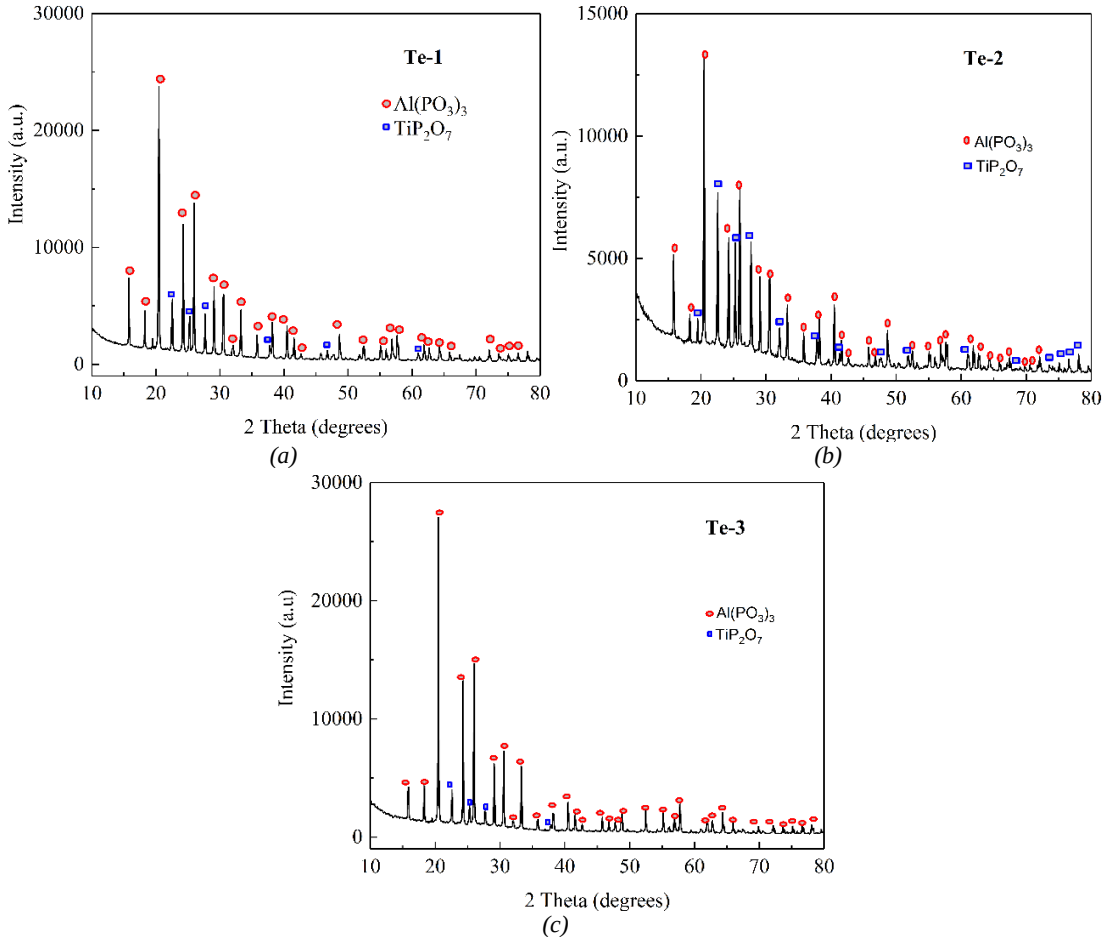

Fig.1. XRD patterns of: a) Te-1; b) Te-2; and c) Te-3 samples (color online)

Table 2 presents the crystallite sizes from the samples: a) Te-1; b) Te-2 and c) Te-3, calculated by means of equation (1), taking into consideration the first seven XRD peaks with descending intensity. The resulted values have been arithmetically mediated.

Figs. 2a, b and c present the FTIR spectra of Te-1, Te-2 and Te-3 crystalline materials, in the range 400-1500 cm^{-1}.

Table 2. Crystallite sizes from Te-1, Te-2 and Te-3 samples, obtained from XRD-data using the Scherrer formula

Te-1			**Te-2**			**Te-3**		
2θ	**D (nm)**	**Average size (nm)**	**2θ**	**D (nm)**	**Average size (nm)**	**2θ**	**D (nm)**	**Average size (nm)**
18.96	18.75	**15.72**	15.88	10	**10.36**	15.77	11.59	**9.07**
18.85	16.42		20.46	10.56		20.35	9.92	
26.21	15.16		24.31	9.71		22.54	10	
27.21	13.66		25.99	10.53		24.22	7.58	
28.18	15.86		29	11.31		25.99	8.67	
31.29	15.23		33.15	10.29		27.76	8.57	
38.37	14.96		38.32	10.12		30.57	7.18	

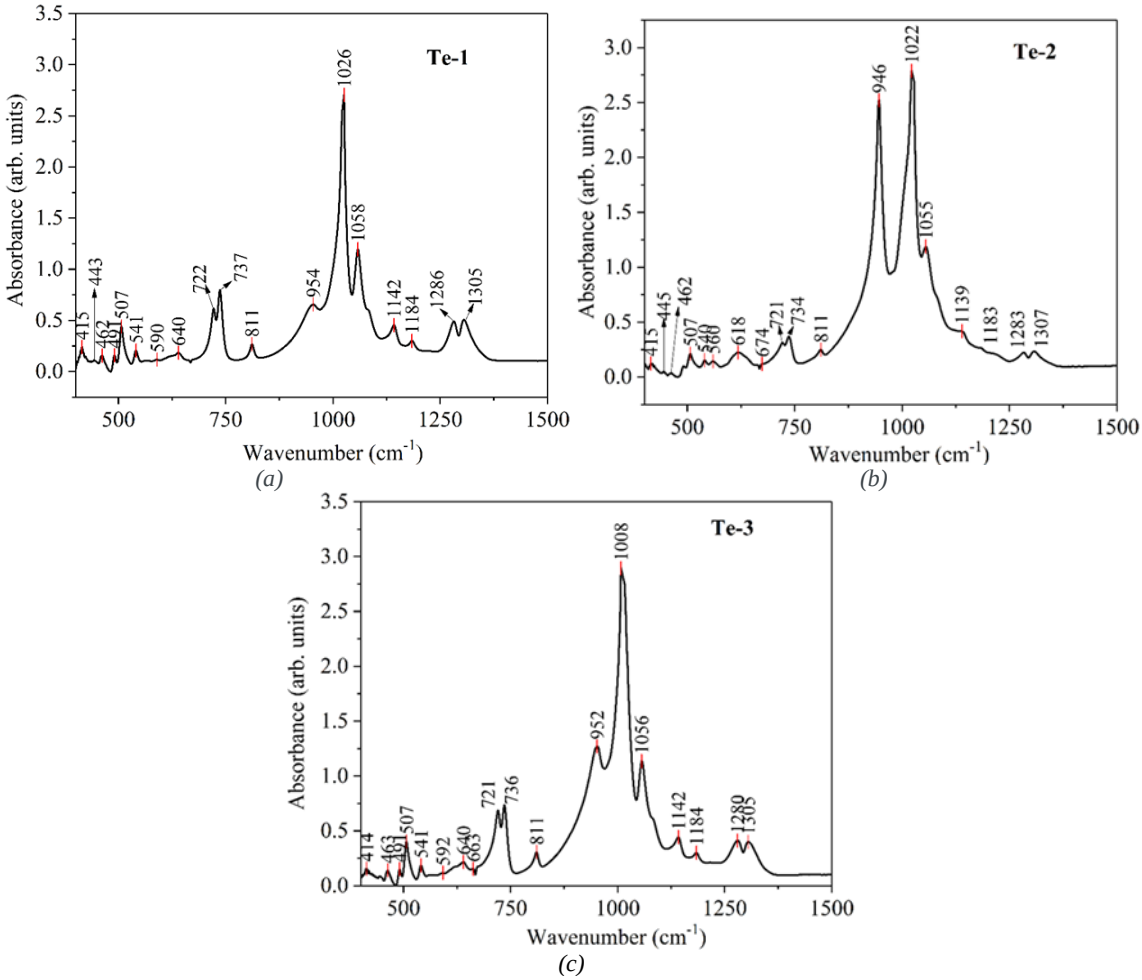

Fig. 2. FTIR spectra of: a) Te-1; b) Te-2; and c) Te-3 samples (color online)

4. Discussions

In the case of Te-1, Te-2, and Te-3 samples (Figs. 1a, b and c), XRD patterns disclosed as crystalline compounds: aluminum metaphosphate, $Al(PO_3)_3$ (Al_2O_3 $3P_2O_5$), as majority phases and titanium pyrophosphate, TiP_2O_7. This is to be expected taking into consideration the high amount of P_2O_5 and the high crystallization tendency of aluminum metaphosphate. The change of the oxide composition (TiO_2: 5-10 mol. %, Al_2O_3: 10-20 mol. % and P_2O_5: 65-75 mol. %, TeO_2 being 5 mol. % constant for all samples) does not affect the crystalline phase formation.

From Fig.1, it is noticed that no tellurium-containing crystalline phases are found in the samples Te-1, Te-2 and Te-3, respectively. TeO_2 could be present in different crystalline phases but under the detection limit of the XRD device, usually 5 %. It is seen from Table 1, that the TeO_2 amount in Te-1, as well as in Te-2 and Te-3 samples, is 5 mol. %. The average crystallite size is ranging between 9-15 nm (see Table 2), in strong correlation with the nucleation and crystallization mechanisms as well as the activation energy of these mechanisms, specific to each heat-treated oxide composition as presented in Table 1 [21-23]. It is noticed a decrease of the nanocrystals average size from Te-1 to Te-3 sample depending on synthesis parameters and oxide composition.

FTIR absorption bands in the case of Te-1, Te-2, and Te-3 samples (Figs. 2a, b, and c), are assigned to Te-O bending and stretching vibration modes from TeO_3, TeO_{3+1} and TeO_4 structural units, in the range 400-670 cm^{-1}. In the case of Te-1, Te-2 and Te-3 samples, the bending vibration modes from the phosphate network, in the range 500-650 cm^{-1} are overlapping the vibration modes from the tellurite network. Typical stretching vibration modes of the phosphate network are evidenced in the range 750 – 1300 cm^{-1}, in the case of Te-1, Te-2 and Te-3 samples.

In Table 3, the assignment of FTIR bands from the investigated crystalline materials is presented.

Table 3. Assignment of FTIR bands from the phosphate-tellurite crystalline materials

Peak assignment/Reference materials/Glass-ceramics	Pure P_2O_5 glass/crystal [21]	Phosphate glasses [21-28]	Tellurite glasses [29-32]	Te-1	Te-2	Te-3
$\delta_{(Te-O-Te)}$; $\delta_{(O-Te-O)}$	-	-	366-484 [30]; 280-550 [31];	415; 443; 462; 491; 507; 541	415; 445; 462; 507; 540; 560;	414; 463; 491; 507; 541;
$\delta_{(O-P-O)}$ and $\delta_{(O=P-O)}$ (phosphate polyhedra)	500 c, g; 475 g; 600 c; 650-680 g; 470 g, 530 g	-	-	507; 541; 590; 640	507; 540; 560; 618	507; 541; 592;
ν_{Te-O} in TeO_4 tbp (trigonal bypiramide)	-	-	600-650 [29]; 594-630 [30]; 560-870 [31]; 665 [32];	640	618	640
$\nu_{(TeO4)}$	-	-	611 [30];	-	618	
ν_{Te-O} in TeO_3 tp (trigonal pyramide)/TeO_{3+1}	-	-	650-700 [29]; 560-870 [31]; 665 [32];	640	674;	640; 663
Te-O vibrations in TeO_4	-	-	664-667 [30];	640	674;	640; 663
Te-O vibrations in TeO_3	-	-	740-758 [30];	737	721; 734;	721; 736
$\nu_{(TeO3)asym}$	-	-	773 [31];	-	-	-
$\nu_{(P-O-P)sym}$ (between Q^1 and Q^2 units)	700-730 c, g; 650 g; 530 g; 780 g	758-700 [21]; 900, 700, [22, 23]; 915- 880 [24]; 780-730 [25]; 710 [28]; 767 [28]	-	640; 722; 737	721; 734;	721; 736;
$\delta_{(P-O-P)}$	910-940 c; 915 g; 780 g; 800-870 c, 780 g	448-570 [21]; 565-495 [25], 487 [28]; 540 [28]; 615 [28]	-	811;	811;	811;
$\delta_{(P-O-H)}$	-	910-850 [21], [22], [23]; 930-915 [25]	-	954	946;	952
$\nu_{(P-O-P)asym}$	-	918 [28]	-	954	946	952
$\nu_{(PO4)^{3-}sym}$ (Q^0 units)/$\nu_{(P2O7)^{4-}sym}$	1015 (+15) c; 1015 g; 1100 g; 930 g; 1040 g	1024-940 [21]; 1100-1040 [26]; 1082-980 [22], [23]; 1025-940 [24]; 1015 [28];	-	954; 1026; 1058	946; 1022;	952; 1008; 1056;
$\nu_{(P-O)^-}$	1120 g (slab)	1136-1120 [22]; 1036-1030 [24]; 1050 [27]; 1100 [22], [23];	-	1026; 1058;	1022; 1055;	1056

Peak assignment/Reference materials/Glass-ceramics	Pure P_2O_5 glass/crystal [21]	Phosphate glasses [21-28]	Tellurite glasses [29-32]	Te-1	Te-2	Te-3
		1110 [26]				
$\nu_{(PO3)^{2-}asym}$	-	1122 [28]; 1158 [28]	-	1142; 1183;	1139; 1183;	1142; 1184
$\nu_{(PO2)^{-}asym}$		1262 [28]				
$\nu_{(P=O)sym}$ **(long phosphate chains)**	1240-1270 c, g; 1285 g; 1230-1300 c; 1390 g; 1240 g	1288-1216 [21]; 1240, 1220 [27]; 1280-1250 [24]; 1282-1205 [26]; 1300-1200 [22], [23]	-	1286; 1305	1283; 1307;	1280; 1305

σ= bending vibration mode
ν=stretching vibration mode
c= crystal
g= glass

Al-O FTIR optical phonons are situated at 470 cm^{-1}, 500 cm^{-1}, 600 cm^{-1}, 650 cm^{-1} and 790 cm^{-1} [33], overlapping P-O and Te-O absorption bands from the investigated samples. According to [34, 35], FTIR absorption bands corresponding to Ti-O and Ti-O-Ti bonds are situated at: 430 cm^{-1}, 440 cm^{-1}, 458 cm^{-1} and 500 cm^{-1}, overlapping Te-O absorption bands from Te-1, Te-2 and Te-3 samples.

The FTIR bands from 954 cm^{-1} and 952 cm^{-1}, in the case of Te-1 and Te-3 samples, respectively, are less intense than that from 946 cm^{-1} in the case of Te-2 sample. This is due to the high amount of P_2O_5, in the case of Te-2 samples compared to Te-1 and Te-3 samples that result in a higher amount of ortho/pyrophosphate compounds.

5. Conclusions

Phosphate-tellurite crystalline materials containing TiO_2 and Al_2O_3 have been synthesized by a wet non-conventional route of the starting reagent processing. Crystalline phases as $Al(PO_3)_3$ and were found to compose the network of the samples. The crystallite size is ranging between 9-15 nm as calculated from XRD patterns, being dependent on the oxide composition and synthesis parameters. Structural information provided by FTIR analysis, proved the crystalline network forming role of P_2O_5 and TeO_2. Bending and stretching vibration modes specific to the phosphate and tellurite network were revealed.

Acknowledgements

This work was supported by UEFISCDI (Executive Unity for Financing of Higher Education, Research and Innovation), Core Program, contracts no. 16N/2019, 18N/2019, 21N/2019 and contracts 47PCCDI/2018 and 42PCCDI/2018.

References

[1] M. Hongisto, A. Veber, N.G. Boetti, S. Danto, V. Jubera, L. Petit, Ceram. Int. **46**(16) Part B, 26317 (2020).
[2] R. Sen, N. N. G. Boetti, M. Hokka, L. Petit, J. Non-Cryst. Solids X **1**, 100003 (2019).
[3] A. Nommeots-Nomm, N. G. Boetti, T. Salminen, J. Massera, M. Hokka, L. Petit, J. Alloy. Compd. **751**, 224 (2018).
[4] R. Narro-García, H. Desirena, T. López-Luke, J. Guerrero-Contreras, C.K. Jayasankar, R. Quintero-Torres, E. De la Rosa, Opt. Mater. **46**, 34 (2015).
[5] L. C. Bolundut, V. Pop, Studia UBB Chemia, **LXI**(4), 223 (2016).
[6] S. V. Stefanovsky, O. I. Stefanovsky, M. I. Kadyko, B. S. Nikonov, J. Nucl. Mater. **500**, 153 (2018).
[7] A. Moguš-Milanković, A. Šantić, L. Pavić, K. Sklepić, Croat. Chem. Acta **88**(4), 553 (2016).
[8] L. Bolundut, P. Pascuta, E. Culea, M. Bosca, L. Pop, R. Stefan, J. Mater. Sci. **55**(23), 9962 (2020).
[9] P. Pascuta, L. Pop, R. Stefan, L. Olar, G. Borodi, L. C. Bolundut, E. Culea, J. Alloy. Compd. **799**, 442 (2019).
[10] Z. X. Hou, H. X. Li, S. H. Wang, M. H. Wang, X. D. Hu, Adv. Mat. Res. **989-994**, 305 (2014).
[11] A. Bertrand, J. Carreaud, S. Chenu, M. Allix, E. Véron, J.-R. Duclère, Y. Launay, T. Hayakawa, C. Genevois, F. Brisset, F. Célarié, P. Thomas, G. Delaizir, Adv. Opt. Mater. **4**(10), 1481 (2016).
[12]. Q. Wei, C. Ma, M. Zhao, G. Ren, C. Su, J. Opt. Adv. Mater., **22**(3-4), 182 (2020).
[13]. M. Zhou, Q. Zhang, F. Tan, J. Chen, Z. Sun, Opt. Adv. Mater. Rap-Comm., Optoelectron. Adv. Mat., **13** (11-12), 609 (2019).
[14] M. Ennouri, I. Jlassi, E. Habib, G. Bernard, J. Lumin. **216**, 116753 (2019).
[15] M. Lesniak, J. Zmojda, M. Kochanowicz, P. Miluski,

A. Baranowska, G. Mach, M. Kuwik, J. Pisarska, W. A. Pisarski, D. Dorosz, Materials **12**(20), 3429 (2019).
[16] M. Elisa, L. Boroica, B. A. Sava, S. M. Iordache, A.-M. Iordache, I. C. Vasiliu, R. C. Stefan, A. C. Galca, V. Kuncser, M. Eftimie, J. Am. Ceram. Soc. **103**(7), 3978 (2020).
[17] M. Elisa, R. C. Stefan, I. C. Vasiliu, S. M. Iordache, A.-M. Iordache, B. A. Sava, L. Boroica, M. C. Dinca, A. V. Filip, A. C. Galca, C. Bartha, N. Iacob, M. I. Rusu, M. Eftimie, V. Kuncser, Nanomaterials **10**(9), 1875 (2020)
[18] M. Elisa, S.M. Iordache, A.-M. Iordache, I. C. Vasiliu, B. A. Sava, L. Boroica, M. C. Dinca, A. V. Filip, A. C. Galca, C. Bartha, V. Kuncser, M. Eftimie, Optoelectronics into a powerful economy, Book of Proceedings, Chapter III. Optoelectronics and optospintronics-emergent phenomena, AGIR Publishing House, Bucharest, 135 (2020)
[19] PDF-ICDD, Powder Diffraction File (PDF-4+ 2018 Software 4.18.0.2); International Centre for Diffraction Data, 12 Campus Boulevard: Newtown Square, PA, USA, 2011
[20] A. L. Patterson, Phys. Rev. **56**(10), 978 (1939).
[21] C. Dayanand, G. Bhikshamaiah, V. Jaya Tyagaraju, M. Salagram, A. S. R. Krishna Murthy, J. Mater. Sci. **31**, 1945 (1996).
[22] D. E. C. Corbridge, E. J. Lowe, J. Chem. Soc. **0**, 493 (1954).
[23] D. E. C. Corbridge, E. J. Lowe, J. Chem. Soc. **0**, 4555 (1954).
[24] R. M. Almeida, J. D. Mackenzie, J. Non-Cryst. Solids **40**(1-3), 535 (1980).
[25] A. A. Higazy, B. Bridge, J. Mater. Sci. **20**, 2345 (1985).
[26] F. A. Miller, C. H. Wilkins, Anal. Chem. **24**(8), 1253 (1952).
[27] R. F. Bartholomew, J. Non-Cryst. Solids **7**(3), 221 (1972).
[28] D. Muresan, M. Dragan Bularda, C. Popa, L. Baia, S. Simon, Rom. J. Phys. **51**(1–2), 231 (2006).
[29] M. K. Halimah, M. F. Faznny, M. N. Azlan, H. A. A. Sidek, Results Phys. **7**, 581 (2017).
[30] S. H. Elazoumi, H. A. A. Sidek, Y. S. Rammah, R. El-Mallawany, M. K. Halimah, K. A. Matori, M. H. M. Zaid, Results Phys. **8**, 16 (2018).
[31] K. M. Kaky, G. Lakshminarayana, S. O. Baki, I. V. Kityk, Y. H. Taufiq-Yap, M. A. Mahdi, Results Phys. **7**, 166 (2017).
[32] G. Lakshminarayana, K. M. Kaky, S. O. Baki, A. Lira, Priyanka Nayar, I. V. Kityk, M. A. Mahdi, J. Alloy. Compd. **690**, 799 (2017).
[33] V. G. Gilev, Inorg. Mater. **37**(10), 1041 (2001).
[34] T. Mahalingam, C. Selvakumar, E. Ranjith Kumar, T. Venkatachalam, Phys. Lett. A **381**(21), 1815 (2017).
[35] J. Yu, X. Zhao, J. C. Yu, G. Zhong, J. Han, Q. Zhao, J. Mater. Sci. Lett. **20**(18), 1745 (2001).

*Corresponding author: ana.filip@inflpr.ro